Adaptive numerical methods for an hydrodynamic problem arising in magnetic reading devices

I. Arregui[1], J. J. Cendán[2], C. Vázquez[3]

Abstract

The mechanical behavior of magnetic reading devices is mainly governed by compressible Reynolds equations when the air bearing modeling approximation is considered. First, the convection dominated feature motivates the use of a characteristics scheme adapted to steady state problems. Secondly, a duality method to treat the particular nonlinear diffusion term is applied. A piecewise linear finite element for spatial discretization has been chosen. Moreover, in certain conditions and devices, strong air pressure gradients arise locally, either due to a strongly convection dominated regime or to the presence of slots in the storage device, for example. In the present work we improve the previous numerical methods proposed to cope with this new setting. Thus, mainly adaptive mesh refinement algorithms based on pressure gradient indicators and appropriate multigrid techniques to solve the linear systems arising at each iteration of the duality method are proposed. Finally, several examples illustrate the performance of the set of numerical techniques.

Key words: Magnetic storage devices, hydrodynamic lubrication, nonlinear Reynolds equation, finite elements, duality methods, multigrid

1. Introduction

In magnetic reading devices, the gap between the reading head and the disk (or tape) where the information is stored has a determining effect on the quality of the stored/received signal. Figure 1 shows the scheme of a general device in which a tape moves over the reading head, both of them separated by a thin air layer. In the case of flexible storage devices, there exists a coupling between the air bearing pressure and the transverse deflection of the tape, thus leading to the formulation of a highly nonlinear elastohydrodynamic coupled problem.

Nevertheless, when the storage device can be assumed to be rigid, such as for example in the case of a computer hard disk, the mechanical problem can be framed into hydrodynamic lubrication theory [7]. In this case, air lubrication between the rotating disk and the slider results to be critical to maintain the optimal gap. In this setting, the adequate mathematical modeling and numerical simulation techniques of the mechanics that are involved in the process provide a very useful tool to evaluate different alternative designs of the devices, preventing from the

[1]Dpto. de Matemáticas, Universidad de La Coruña, Facultad de Informática, Campus de Elviña, E-15071 La Coruña. E-mail: arregui@udc.es

[2]Dpto. de Matemáticas, Universidad de La Coruña, Facultad de Informática, Campus de Elviña, E-15071 La Coruña. E-mail: suceve@udc.es

[3]Dpto. de Matemáticas, Universidad de La Coruña, Facultad de Informática, Campus de Elviña, E-15071 La Coruña. E-mail: carlosv@udc.es

costs associated to build them.

Concerning the mathematical modeling, different modified Reynolds equations have been proposed in the literature, the departure point being the consideration that the gap size is smaller than the molecular free path, so that the usual continuum theory is no longer valid and rarefaction effects have to be taken into account. Among the different alternatives of compressible Reynolds equations corresponding to different situations, in [8] the so called first order slip correction model we consider in the present paper was first proposed. The mathematical analysis of different compressible Reynolds equations in two spatial variables for L^∞ gap functions has been addressed in [9]. Previously, in [11, 12] the case of one spatial variable the analysis of flexible device where the first order compressible Reynolds equation is coupled with an elastic model. More precisely, in [11] a case with regular gap functions is treated and in [12] the presence of head slots leads to discontinuous gap functions.

Concerning the numerical methods, in the case of smooth gap functions different strategies have been proposed in the literature. For example, in [18] a finite differences scheme for a coupled model is proposed, in [16] a LPDEM discretization scheme combined with a Newton-Raphson technique for the discretization of compressible Reynolds equation is applied. More recently, in [2] a duality method based on maximal monotone operators for the nonlinear diffusive term arising in compressible Reynolds equation is considered. Moreover, this method is combined with a characteristics scheme adapted to steady state problems to treat the convection dominating feature of the equation in real devices and piecewise linear Lagrange finite elements for spatial discretization are used. Despite the theoretical analysis developed in [1] in one spatial dimension, this joint strategy has shown a good behavior in the case of smooth gap functions (even in case that they are highly oscillating functions due to the presence of periodic roughness in the surfaces in contact) and in two spatial dimensions when coupled with elastic models in flexible read devices (see [2]).

Nevertheless, the assumption of smooth gap sometimes results to be very restrictive. In many devices some slots are introduced to reduce the air pressure and improve the reading conditions [10]. The mathematical analysis of models including discontinuous gap functions has been developed in [12] and some numerical experiences are shown in [23]. More particularly, in the case of hard disk drives, the etching technique in the manufacturing process produces a steep narrow wall gap region along the rail boundaries (see [22], for example). The discontinuous or rapid changing gap geometry leads to very large pressure gradients either near the slots or near the large gap function gradients. In this setting, in order to obtain sufficiently accurate results in the computed magnitudes during simulation, the use of appropriate numerical schemes and meshing techniques is required. In [22] an adaptive technique is applied to a numerical method based on an upwind finite volume scheme for the convection term combined with a Galerkin weighed integral for the diffusion term, the resulting nonlinear discretized problem being solved by an explicit treatment of the pressure in the nonlinear term (that is, a kind of fixed point iteration termed as lagging technique in [22]). Moreover, a multigrid technique for the linear discretized problem is proposed and an imposed load problem to obtain the unknown gap coefficients is posed. More recently, in [14] an adaptive finite element strategy is proposed for a hard disk drive simulation, the mesh refinement criteria being based on the size of the pressure and gap gradients.

In the present work, we propose an adaptive refinement technique to apply the numerical

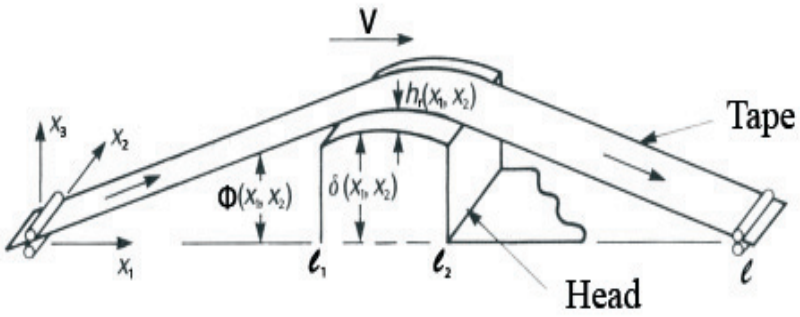

Figure 1: Schematic example of a magnetic recording device.

methods proposed in [2] when slots or large gradients in the gap appear in the simulated devices. Moreover, we propose a multigrid scheme to solve the linear systems that arise at each iteration of the duality algorithm in the solution of the discrete problem. Thus, the plan of the paper is as follows. In section 2 the mathematical model is presented. In Section 3 the main numerical methods and algorithms are described. Section 4 explains the adaptive refinement technique and the multigrid strategy for the linear system solver. In Section 5 several numerical examples to illustrate the performance of the numerical methods. Finally, Section 6 contains the conclusions.

2. Mathematical model

In the first order slip-flow correction model, the behavior of the air pressure p in the thin layer is governed by the following compressible Reynolds equation:

$$\nabla \cdot \left(\frac{h^3 p}{\eta(p)} \right) = 6 \, \frac{\partial}{\partial x_1}(Vph) \qquad \text{in } \Omega = (\ell_1, \ell_2) \times (0, \ell_2 - \ell_1) \,, \tag{1}$$

where h represents the gap between the reading head and the information storage device, V is the constant velocity of the moving head, η denotes the effective viscosity of the air and ℓ_1 and ℓ_2 are related to the physical dimensions of the device (see Fig. 1). Equation (1) is completed with the appropriate Dirichlet boundary condition

$$p = p_a \qquad \text{on} \quad \partial\Omega, \tag{2}$$

where p_a denotes the ambient pressure.

Compressible Reynolds equations are classically used when modeling air bearing lubrication processes such as those appearing in magnetic storage devices. These equations can be deduced either from Navier–Stokes or Stokes ones under some assumptions. More precisely, in order to state Equation (1) a constant velocity of the device is considered, the effects of the surface stresses are neglected and the air behavior as a perfect gas is assumed, so that the density is proportional to pressure. Moreover, as in other thin layer settings, we also assume that the air layer width is much smaller than the other dimensions, Also, we neglect the inertial forces compared to the viscosity forces. Under previous assumptions, recently in [19] a rigorous derivation of a compressible Reynolds equation from the compressible Navier-Stokes system by using asymptotic analysis techniques is obtained. The analogous derivation of linear Reynolds equation is contained in the classical paper [3] and a recent review on the state of art in mathematical

modeling and numerical methods in lubrication appears in [4].

In (1) the effective viscosity of the air can be expressed as [7]:

$$\eta(p) = \frac{\eta_a}{1+\gamma/(ph)}\,, \tag{3}$$

where η_a denotes the constant viscosity at ambient conditions and $\gamma = 6aMp_ah_m$, a being a surface correction coefficient, $M = \lambda/h_m$ the Knudsen number at ambient pressure, λ the local mean free path and h_m the reference film thickness. Thus, replacing expression (3) in equation (1) we get

$$\nabla\cdot\big((\gamma h^2 + h^3 p)\nabla p\big) = 6V\eta_a\frac{\partial}{\partial x_1}(ph)\,. \tag{4}$$

Under certain hypotheses [9], existence and uniqueness of solution to problem (4) can be obtained, as well as upper and lower L^∞ bounds. More precisely, the following result can be obtained.

Theorem 1 If $h \in L^\infty(\Omega)$ and $0 < h_{\min} \le h \le h_{\max} < \infty$, then equation (4) jointly with boundary condition (2) admits a unique solution $p \in V_a$ such that

$$0 \le p \le R_0\,,$$

where $R_0 = \max\big\{2p_a\,,\, 2h_{\min}^{-3}(2K\,|\Omega|\,h_{\max} - \gamma h_{\min}^2)\big\}$, $K = 0.5\,\|\Omega\|^{1/2}\,s^*\,2^{1/(s^*-2)}$ and $s^* = 2 + \log(2) + \sqrt{4\ln(2) + (\ln(2))^2}$.

The proof of Theorem 1 can be easily obtained from the results stated in [9] and it also has been recently extended to an elastohydrodynamic model for flexible devices in [2].

Next, as a previous step to identify the orders of the different terms involved in equation (4), i.e. advection and nonlinear diffusion, and select the more appropriate numerical methods, we introduce the following scaling in the geometric coordinates and magnitudes [10]:

$$X_1 = \frac{x_1}{\ell}\,, \qquad X_2 = \frac{x_2}{\ell}\,, \quad P = \frac{p}{p_a}\,, \qquad H = \frac{h}{h_m}\,,$$

where ℓ denotes the order of magnitude of the spatial domain. Then, the dimensionless domain is defined by

$$\Omega_H = (L_1, L_2)\times(0, L_2 - L_1)\,, \qquad \text{where } L_i = \ell_i/\ell, \quad i = 1,2,$$

and Equation (4) can be written in the equivalent dimensionless form in the domain Ω_H:

$$\frac{\partial(PH)}{\partial X_1} \; - \nabla\cdot\big((\alpha H^2 + \beta H^3\,P\,)\nabla P\big) = 0\,. \tag{5}$$

In real applications the diffusion coefficients α and β are of a much smaller order than the advection one, so that we are dealing with a convection dominated advection-diffusion equation. Moreover, when $\beta \neq 0$ equation (5) contains a nonlinear diffusive term.

3. Main numerical methods.

In order to overcome the difficulty related to the advection dominated feature, in [2] we propose a characteristics method adapted to steady state problems. For this purpose, we first introduce an artificial dependence on t in the functions P and H, by defining the new functions $\bar{P}$ and $\bar{H}$ as follows:

$$\bar{P}(t,(X_1,X_2)) = P(X_1,X_2), \qquad \bar{H}(t,(X_1,X_2)) = H(X_1,X_2),$$

and we consider the artificial velocity field $\vec{v}(X_1,X_2) = (1,0)$ associated to the particular expression of the convection term in (5). Then, the convection term can be written as

$$\frac{\partial(PH)}{\partial X_1} = \frac{D(\bar{P}\bar{H})}{Dt}\,,$$

where

$$\frac{D(\bar{P}\bar{H})}{Dt} = \frac{\partial(\bar{P}\bar{H})}{\partial t} + v\cdot\nabla(\bar{P}\bar{H})$$

denotes the material derivative of function $\bar{P}\bar{H}$. Next, we introduce the characteristic curve associated to the velocity field $\vec{v}$ through the point (X_1,X_2) at time t, which is parameterized in the time variable τ as

$$\tau \longrightarrow \chi((X_1,X_2),t;\tau).$$

Notice that the function $\chi((X_1,X_2),t;\cdot)$ is the solution of the following first order ODE Cauchy problem:

$$\begin{cases} \dfrac{d\chi}{d\tau}((X_1,X_2),t;\tau) = v(\chi((X_1,X_2),t;\tau))\,, \\ \chi((X_1,X_2),t;t) = (X_1,X_2)\,. \end{cases}$$

Next, we introduce an *artificial* time step k and we approximate the material derivative at the point $(t,(X_1,X_2))$ by the upwinded quotient:

$$\begin{aligned} \frac{D(\bar{P}\bar{H})}{Dt}(t,(X_1,X_2)) &\approx \frac{(\bar{P}\bar{H})(t,(X_1,X_2)) - (\bar{P}\bar{H})(\chi((X_1,X_2),t;t-k)}{k} \\ &= \frac{(PH)(X_1,X_2) - (PH)(t,\chi^k(X_1,X_2))}{k}\,. \end{aligned} \tag{6}$$

For the particular velocity field $\vec{v}$ we have that $\chi^k(X_1,X_2) = \chi((X_1,X_2),t;t-k) = (X_1-k,X_2)$. Thus, after introducing the approximation (6) in (5), the algorithm of the characteristic method for the steady state can be posed. More precisely, starting from P_0, for a given P_m at step m, we obtain P_{m+1}, such that:

$$P_{m+1}H - k\nabla\cdot\left(\alpha H^2\nabla P_{m+1}\right) - k\nabla\cdot\left(\beta H^3 P_{m+1}\nabla P_{m+1}\right) = (P_m H)\circ\chi^k\,. \tag{7}$$

Notice that the elliptic equation (7) still contains a nonlinear diffusive term. Following the ideas in [2] we treat this nonlinearity by using a duality method. For this purpose, let us introduce the maximal monotone operator f, defined by

$$f(P) = \begin{cases} 0 \quad , & \text{if } P<0, \\ P^2 \quad , & \text{if } P\geq 0, \end{cases}$$

so that

$$P_{m+1}\nabla P_{m+1} = \frac{1}{2}\nabla\left(f(P_{m+1})\right).$$

Therefore, a variational formulation associated to (7) can be written in the form:

Find $P_{m+1} \in V_a$, such that:

$$\int_{\Omega_H} P_{m+1} H\, \varphi + k\alpha \int_{\Omega_H} H^2 \nabla P_{m+1} \nabla \varphi + \\ + \frac{k\beta}{2} \int_{\Omega_H} H^3 \nabla \left(f(P_{m+1}) \right) \nabla \varphi = \int_{\Omega_H} \left((P_m H) \circ \chi^k \right) \varphi \,, \ \forall \varphi \in V_0 \tag{8}$$

where the involved functional and set spaces are

$$V_a = \left\{ \varphi \in H^1(\Omega) \,/\, \varphi = p_a \ \text{ on } \partial\Omega \right\} ,$$
$$V_0 = \left\{ \varphi \in H^1(\Omega) \,/\, \varphi = 0 \ \text{ on } \partial\Omega \right\} .$$

Following the duality technique introduced in [6], in terms of the constant parameter $\omega > 0$ we introduce the new additional unknown θ_{m+1}, defined by

$$\theta_{m+1} = (f - \omega I)(P_{m+1}),$$

where I denotes the identity operator. Thus, we get

$$f(P_{m+1}) = \theta_{m+1} + \omega P_{m+1}, \qquad \nabla \left(f(P_{m+1}) \right) = \nabla \theta_{m+1} + \omega \nabla P_{m+1}.$$

Then, the couple (P_{m+1}, θ_{m+1}) is the solution of the nonlinear problem:

$$(\mathcal{P}_m) \begin{cases} \displaystyle\int_{\Omega_H} P_{m+1} H\, \varphi + k\alpha \int_{\Omega_H} H^2 \nabla P_{m+1} \nabla \varphi + k \frac{\beta\omega}{2} \int_{\Omega_H} H^3 \nabla P_{m+1} \nabla \varphi = \\ \qquad = \displaystyle\int_{\Omega_H} \left((P_m H) \circ \chi^k \right) \varphi - \frac{k\beta}{2} \int_{\Omega_H} H^3 \nabla \theta_{m+1} \nabla \varphi \,, \qquad \forall \varphi \in V_0, \\ \\ \theta_{m+1} = f(P_{m+1}) - \omega P_{m+1}, \end{cases}$$

which is equivalent to (8). Next, by using the Bermúdez–Moreno lemma stated in [6], we have the equivalence

$$\theta_{m+1} = f(P_{m+1}) - \omega P_{m+1} \qquad \Longleftrightarrow \qquad \theta_{m+1} = f_\lambda^\omega (P_{m+1} + \lambda \theta_{m+1}) \,,$$

where f_λ^ω denotes the Yosida approximation of $f - \omega I$. For convergence purposes, in the choice of the parameters λ and ω we impose the relation $2\lambda\omega = 1$. Under this constraint, the Yosida approximation can be analytically computed and is given by

$$f_{\frac{1}{2\omega}}^\omega \left(P + \frac{\theta}{2\omega} \right) = \begin{cases} -\theta - 2\omega P \quad , & \text{if } P + \dfrac{\theta}{2\omega} \leq 0, \\ \\ \theta + 2\omega P + \omega^2 - \omega \sqrt{4\theta + 8\omega P + \omega^2} \quad , & \text{if } P + \dfrac{\theta}{2\omega} \geq 0. \end{cases}$$

By taking into account the previous results, at each step of the characteristic algorithm the following fixed–point algorithm to approximate the solution of problem $(\mathcal{P}_m)$ for $m = 0, 1, \ldots$ can be applied:

- Let P_0 be a given initial pressure

- For $m = 0,\ 1,\ 2, \ldots$
  - We obtain the term $(P_m H) \circ \chi^k$
  - For $j = 1, 2, \ldots$

    For a given θ^j_{m+1} we obtain $P^{j+1}_{m+1} \in V_a$ by solving

$$\int_{\Omega_H} P^{j+1}_{m+1} H \varphi + k \int_{\Omega_H} \left(\alpha H^2 + \frac{\beta \omega H^3}{2} \right) \nabla P^{j+1}_{m+1} \nabla \varphi = \\ = \int_{\Omega_H} \left((P_m H) \circ \chi^k \right) \varphi - \frac{k\beta}{2} \int_{\Omega_H} H^3 \nabla \theta^j_{m+1} \nabla \varphi \,, \qquad \forall \varphi \in V_0 \tag{9}$$

    We update θ^j_{m+1} by using the identity

$$\theta^{j+1}_{m+1} = f^{\omega}_{1/2\omega} \left(P^{j+1}_{m+1} + \frac{1}{2\omega} \theta^j_{m+1} \right)$$

  - We check the stopping test in the duality algorithm
- We check the stopping test in the characteristics algorithm.

For the spatial discretization of the linear problem (9), piecewise linear Lagrange finite elements on a triangular mesh have been applied. Moreover, appropriate Gauss formulae for numerical quadrature to compute the different integral terms have been used.

4. Adaptive refinement and linear system solver

As indicated in previous sections, many magnetic storage processes give rise to advection dominated problems, so that very large pressure gradients appear in different regions. In these situations, very fine meshes are necessary in order to attain a good approximation of the pressure values. Moreover, other real devices involve rapidly changing gap functions, even sometimes discontinuous ones as a consequence of the presence of trenches dug into the head. The presence of these slots also produces very high pressure gradients located at irregularly distributed regions, thus requiring again the use of fine enough grids. Although in the present problem the location of gap discontinuities are a priori known, the precise regions with large pressure gradients are unknown. By these reasons, we propose the use of a convenient adaptive technique.

In classical adaptive methods, an error estimator is computed on each element of the finite element mesh. The adaptive meshing algorithm we propose uses the pressure gradient as the metric for the refinement procedure. Thus, after computing the approximated pressure gradient for each element, we just refine the elements where the pressure gradient is larger. More precisely, we compute a norm of the gradient of the pressure, $\eta_e = \mid \nabla P_e \mid$, over all the triangular elements e of the mesh and we just refine the elements that satisfy the condition

$$\eta_e > \eta_{\min} + \rho(\eta_{\max} - \eta_{\min}) \,,$$

where $\rho \in [0, 1)$. This strategy results to be a cheap way to get a better approximation in some specific regions of the domain. As it is also important to refine the mesh locally along the edges of the slots where there is an abrupt change of the gap function which produces very large changes in pressure distribution near those points, another refinement criterium related to the

fact that the element is located near the slot or gap discontinuity is jointly considered.

Once the elements to be refined have been identified according to the previous criterium, each triangle is divided into four subtriangles, the mid-point of the longest side being connected with the opposite vertex and the other two sides mid-points. Next, in order to ensure the conformity of the new mesh, an additional refining step (by subdivision into two or three subtriangles) has to be performed.

At each refinement level we propose a double loop iterative algorithm: at each iteration of the inner (duality) loop, we must solve a system of linear equations. As the global technique sometimes results to be too expensive, we propose to combine the previous adaptive refinement technique with a geometric multigrid method to solve the linear system of equations associated to (9). In this sense, we have been inspired by [15], where a similar technique for a duality method in the frame of obstacle problems is proposed.

Notice that in multigrid algorithms, the intermediate approximations, residuals and corrections have to be transferred between the meshes of different levels. For example, we recall the steps in the classical two grid V–cycle: given an initial approximation $\bar{u}_h^\ell$ of the solution of the linear system $A_h^\ell u_h \ell = b_h^\ell$, we smooth it by means of ν_1 iterations of a relaxation method, which provides an approximation $\hat{u}_h^\ell$. Next, we restrict the residual on the previous coarser mesh $(\ell-1)$ and solve (exactly) the error equation

$$A_h^{\ell-1} w_h^{\ell-1} = \mathcal{R}\left(b_h^\ell - A_h^\ell \hat{u}_h^\ell\right) .$$

Then, we interpolate the error vector $w_h^{\ell-1}$ on the actual finer mesh (ℓ) and correct the previous approximation by using

$$\hat{\hat{u}}_h^{\ell-1} = \hat{u}_h^\ell + \mathcal{P}\left(w_h^{\ell-1}\right) .$$

Finally, we smooth again the approximation (by means of ν_2 iterations of a relaxation method) to get u_h^ℓ. So, we can summarize the previous procedure by writing one multigrid iteration step in the form

$$u_h^\ell = \mathcal{S}^{\nu_2}\left(\hat{u}_h^\ell + \mathcal{P}\left([A_h^{\ell-1}]^{-1}\mathcal{R}\left(b_h^\ell - A_h^\ell \mathcal{S}^{\nu_1}(\bar{u}_h^\ell)\right)\right)\right) ,$$

where $\mathcal{S}$, $\mathcal{P}$ and $\mathcal{R}$ denote the smoothing, interpolation (prolongation) and restriction operators, respectively.

Notice that in the multigrid V–cycle, the previous algorithm is used instead of the exact solution of the system in level $(\ell - 1)$, so that levels $\ell - 1$, $\ell - 2$, ..., $\ell - k$ are involved. Efficiency of these methods has been shown for a wide class of problems [13, 20, 5], including other hydrodynamic lubrication problems [21]. In the present paper we use this scheme to solve equation (9) at each refinement level. The elements of our multigrid method are a lexicographical Gauss–Seidel iteration as smoother and a linear interpolation operator, while the restriction is just an injection from the fine to the coarse mesh.

5. Numerical results

In this Section some numerical tests are shown, in order to show the good behavior of the previous numerical techniques for the simulation of different head–tape recording systems. The first one is a very simple academic test, while the other ones are more realistic. In all test

examples the equations are written in dimensionless form. Having in view the more realistic cases, all the figures are shown in real values corresponding to the scaling parameters $\ell = 0.015\, m$, $p_a = 84100\, Pa$ and $h_m = 10^{-8}\, m$.

Test 1

In this first test, we use the previously described techniques to approximate the function P that satisfies the equation

$$\frac{\partial}{\partial X_1}(PH) - \alpha\nabla\cdot\left(H^2\nabla P\right) - \beta\nabla\cdot(H^3 P\nabla P) = F \qquad \text{in } \Omega_H = (0,1)\times(0,1)$$

jointly with the boundary condition

$$P = 1 \quad \text{ on } \partial\Omega_H\,.$$

The function H is given by $H(X_1, X_2) = 2 - X_1$ and the constant parameters $\alpha = \beta = 3\times 10^{-3}$ have been taken. Moreover, the function F is chosen so that the solution of the problem is $P(X_1, X_2) = 1 + X_1X_2(1 - X_1)(1 - X_2)$.

For the numerical solution, the time discretization step $k = 0.01\Delta X$ has been taken, where ΔX denotes minimum diameter of the elements in the finite element mesh. Moreover, the parameter of the duality method $\omega = 2$ has been chosen. The tolerance for the convergence of the characteristics scheme to the steady state solution and for the convergence of the duality method are both taken equal to 10^{-5}. Moreover, starting from an initial very coarse mesh with 2 triangular elements and 5 nodes, Table 1 shows the number of nodes, the number of elements and the relative quadratic error at the different refinement levels when the parameter $\rho = 0.34$ in the gradient pressure indicator is used.

Level	**NN**	**NE**	**Error**
1	9	8	2.213566×10^{-2}
2	25	32	1.157669×10^{-2}
3	67	108	5.921858×10^{-3}
4	196	254	4.781937×10^{-3}

Table 1: Number of nodes (NN), number of elements (NE) and relative quadratic error (Error) for different levels of refinement in Test1.

Test 2

In this test we consider the compressible Reynolds equation obtained by just replacing $F = 0$ in the previous equation, that is

$$\frac{\partial}{\partial X_1}(PH) - \alpha\nabla\cdot\left(H^2\nabla P\right) - \beta\nabla\cdot(H^3 P\nabla P) = 0$$

Moreover, we consider a domain $\Omega = (0,1)\times(0,1)$ and the same values of α, β, function H and boundary condition that in Test 1. Notice that in this case the solution cannot be computed analytically. Moreover, we refine the mesh in the region where the pressure gradient is larger according to parameter $\rho = 0.34$, the other parameters of the numerical methods being also the same as in Test 1. Table 2 shows the evolution of the number of nodes and elements of

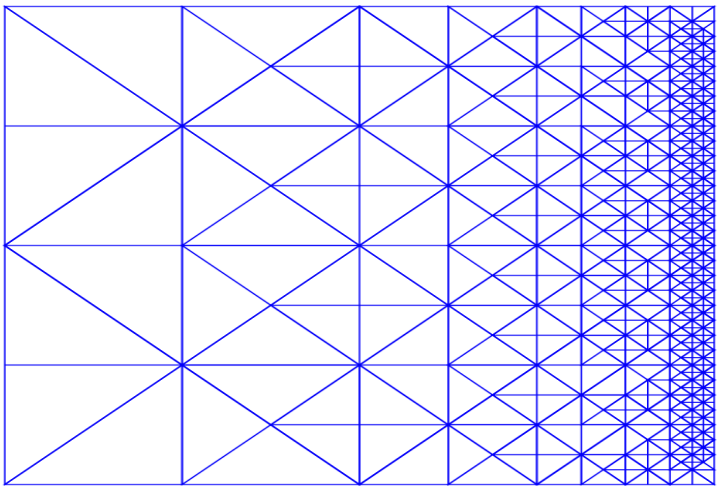

Figure 2: Final mesh after six refinement levels in Test 2.

the meshes obtained during the refinement process. Figure 2 shows the achieved mesh after six refinement levels and Figure 3 shows the computed pressure distribution for this mesh. From both figures we can verify that the mesh is refined where the pressure gradients are larger, this region being located at the right hand side of the domain.

Level	**NN**	**NE**
1	9	8
2	25	32
3	59	92
4	125	212
5	240	422
6	387	688

Table 2: Number of nodes (NN) and number of elements (NE) for different levels of refinement in Test2.

Test 3

In this test we introduce the slots on a flat decreasing gap. More precisely, the gap function is now given by the following discontinuous function defined on $\Omega_H = (0,1) \times (0,1)$:

$$H(X_1, X_2) = \begin{cases} 1.9 & \text{if } (X_1, X_2) \in (0.2, 0.4) \times (0.475, 0.525) \\ 1.6 & \text{if } (X_1, X_2) \in (0.5, 0.7) \times (0.475, 0.525) \\ 2 - X_1 & \text{elsewhere.} \end{cases}$$

Figure 4 shows the gap given by the previous function. The equation is the same as in Test 2 with the same parameters and the refinement criterium involves the pressure and height gradients with the parameter $\rho = 0.34$, the other parameters of the numerical methods being also the same as in Test 1. Table 3 shows the evolution of mesh data along the refinement procedure.

Figure 5 shows the mesh obtained after eight refinement levels. Notice the mesh is mainly refined near the slots and at the regions with large pressure gradients as it can be verified by

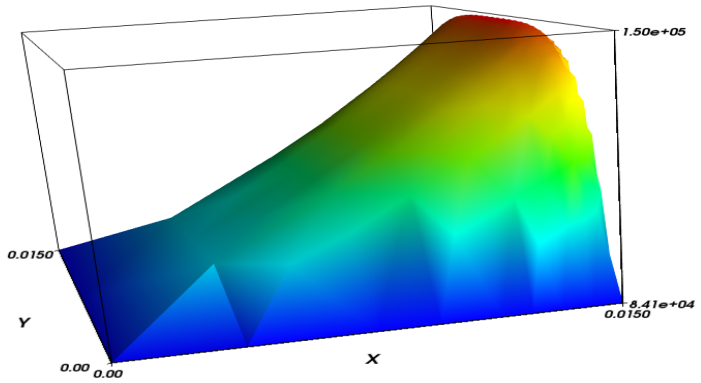

Figure 3: Computed pressure distribution after six refinement levels in Test 2.

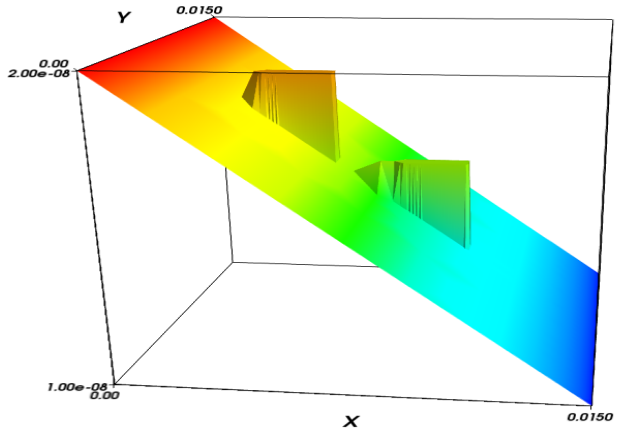

Figure 4: Gap function in Test 3.

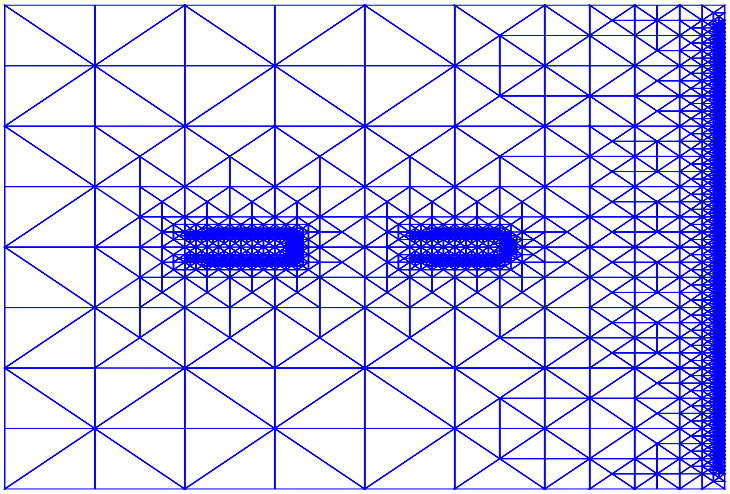

Figure 5: Final mesh after 8 refinement levels in Test 3.

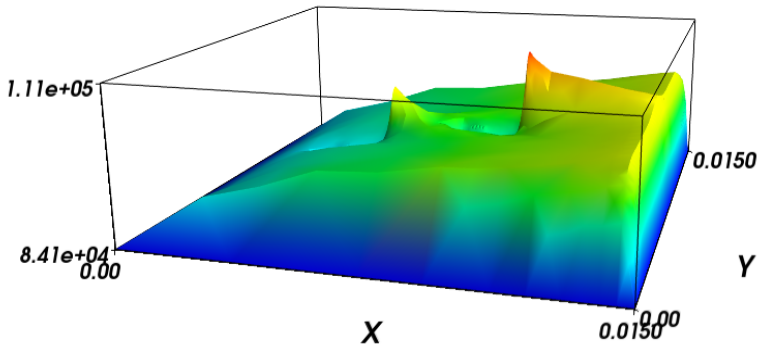

Figure 6: Computed pressure distribution after 8 refinement levels in Test 3.

Level	NN	NE
1	9	8
2	25	32
3	80	92
4	162	126
5	337	278
6	592	608
7	1197	1090
8	2284	4298

Table 3: Number of nodes (NN) and number of elements (NE) for different levels of refinement in Test3.

comparing with Figure 6. The pressure value starts to increase from the left boundary as soon as the gap decreases. Then, the left border of the first slot implies a sudden jump in the gap to a large value along the slot, so that the pressure decreases until the new jump at the end of the slot leads to a sudden increase of the pressure until reaching the next slot that repeats the pressure pattern. At the right hand side a large pressure gradient appears until reaching the ambient pressure at the right boundary.

Test 4

Last test corresponds with a device that includes a cylindrical head with two slots. Numerical examples for this kind of head geometries appear in [23], for example. More precisely, in this test the gap between the head and the tape is defined by the following function in the same domain as Test 3:

$$H(X_1, X_2) = \begin{cases} 1.2 & \text{if } (X_1, X_2) \in (0.2, 0.4)\times(0.475, 0.525) \\ 1.2 & \text{if } (X_1, X_2) \in (0.6, 0.8)\times(0.475, 0.525) \\ 1 + (X_1 - 0.5)^2 & \text{elsewhere.} \end{cases}$$

Figure 7 represents the gap function, this function being the only difference with respect to Test 3, in which a flat surface instead a cylindrical one is considered outside the slots region. In Table 4 the mesh data evolution with refinement are presented.

Level	NN	NE
1	9	8
2	25	32
3	77	122
4	243	426
5	499	920
6	865	1618
7	1544	2928
8	2457	4748
9	4293	8408

Table 4: Number of nodes (NN) and number of elements (NE) for different levels of refinement in Test 4.

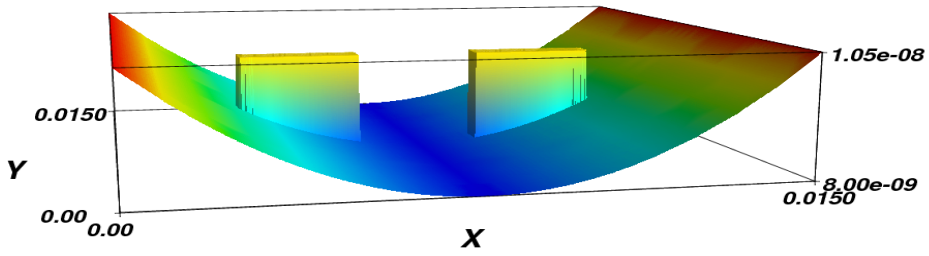

Figure 7: Gap function in Test 4.

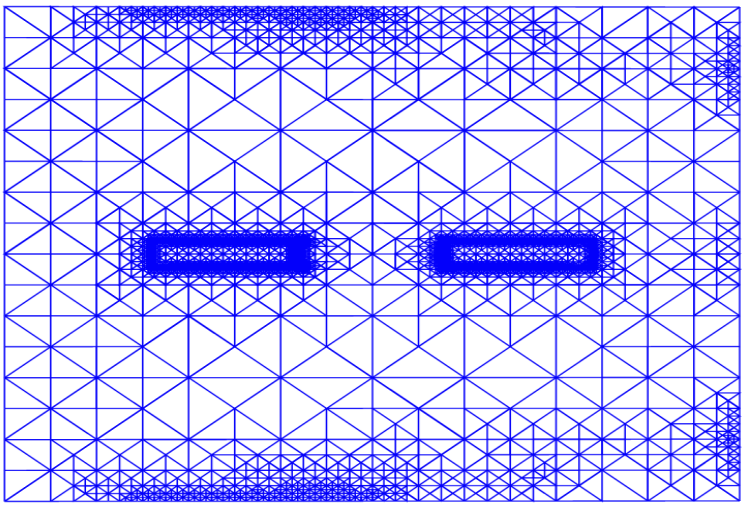

Figure 8: Final mesh after 9 refinement levels in Test 4.

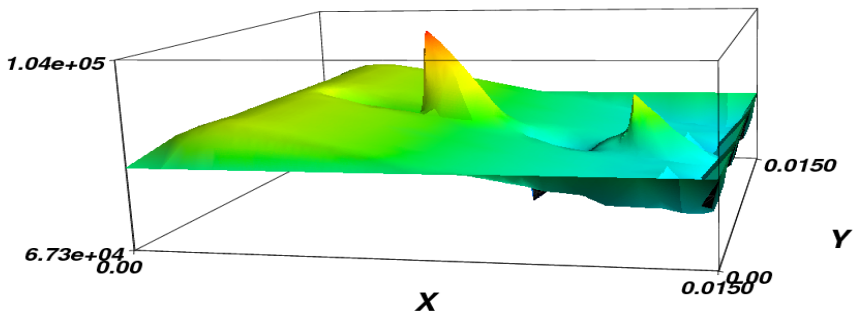

Figure 9: Computed pressure distribution after 9 refinement levels in Test 4.

Figure 8 shows the mesh obtained after nine refinement levels. Notice the mesh is mainly refined near the slots and at larger pressure gradient regions as it can be verified comparing with Figure 6. The qualitative behavior is very close to the one of Test 3, although some specific features arise from the presence of a cylindrical head outside the slots region.

6. Conclusions

In this paper a combination of numerical techniques to simulate the mechanical behavior of magnetic storage device is introduced, mainly focused to the case where the head presents some slots in order to improve the quality of the reading/writing process. More precisely, first the characteristics scheme combined with a duality method and piecewise linear Lagrange finite elements to approximate the solution of the compressible nonlinear Reynolds equation is used. The convection dominated feature jointly with the presence of slots leading to discontinuous functional coefficients give rise to regions with large pressure gradients. Thus, further specific techniques to accurately recover the pressure profile are required. In this paper, an adaptive mesh refinement algorithm to capture the specific aspects of the gap related to the presence of slots, and also the regions of large pressure gradients. The adaptive technique is combined with a multigrid strategy. A first academic test with analytical solution illustrates the convergence of the proposed algorithm. Next, the methods are applied to different devices without and with slots. In the presence of slots, a flat and a cylindrical reading head have been considered.

This methodology can be extended in the future to other rigid devices, such as real hard disks in computers. Moreover, the set of techniques can be applied in the setting of flexible devices previously treated by the authors in the case without slots. Also the hydrodynamic or elastohydrodynamic problem with imposed load can be addressed. In this case, some unknown parameters appearing in the gap function are identified by imposing a prescribed load to the device.

Aknowledgments

This paper has been partially founded by Spanish MCINN (Project MTM2010–21135–C02–01) and Xunta de Galicia (Project INCITE09-105-339-PR and Ayuda CN2011/004 cofinanced with FEDER funds).

References

[1] I. Arregui, J. J. Cendán, C. Parés, C. Vázquez, *Numerical simulation of a 1-d elastohydrodynamic problem in magnetic storage devices*, ESAIM Math. Model. Numer. Anal., **42** (2008) 645–665.

[2] I. Arregui, J. J. Cendán, C. Vázquez, *Numerical simulation of head/tape magnetic reading devices by a new 2-D model*, Finite Elements Anal. Des., **43** (2007) 311–320.

[3] G. Bayada, M. Chambat, *The transition between the Stokes equation and the Reynolds equation: a mathematical proof*, Applied Mathematics and Optimization, **14** (1986) 73–93.

[4] G. Bayada, C. Vázquez, *A survey on mathematical aspects of lubrication problems*, Boletín SeMA, **39** (2007) 31–74.

[5] A. Brandt, C. W. Cryer, *Multigrid algorithms for the solution of linear complementarity problems arising from free boundary problems*, SIAM J. Sci. Stat. Comput., **4** (1983), 655–684.

[6] A. Bermúdez, C. Moreno, *Duality methods for solving variational inequalities*, Comput. Math. Appl., **7** (1981) 43–58.

[7] B. Bhushan, *Tribology and Mechanics of Magnetic Storage Devices*, Springer, New York, 1996.

[8] A. Burgdorfer, *The influence of the molecular mean free path on the performance of hydrodynamic gas lubricated bearings*, ASME Journal of Basic Engineering, **81** (1959) 94–100.

[9] G. Buscaglia, S. Ciuperca, M. Jai, *Existence and uniqueness for several nonlinear elliptic problems arising in lubrication theory*, J. Differ. Eq., **218** (2005) 187–215.

[10] A. Friedman, *Mathematics in Industrial Problems*, **7**, Springer, New York, 1995.

[11] A. Friedman, B. Hu, *Head–media interaction in magnetic recording*, Arch. Rational Mech. Anal., **140** (1997) 79–101.

[12] A. Friedman, J. I. Tello, *Head–media interaction in magnetic recording*, J. Differ. Eq., **171** (2001) 443–461.

[13] W. Hackbusch, *Multigrid Methods and Applications*, Springer, 1985.

[14] P. Holani, S. Müftü, *An adaptive finite element strategy for analysis of air lubrication in the head-disk interface of a hard disk drive*, Revue Européenne des Éléments Finis, **14** (2005) 155–180.

[15] R. H. W. Hoppe, *Multigrid methods for variational inequalities*, SIAM J. Numer. Anal., **24** (1987) 1046–1065.

[16] M. Jai, *Homogenization and two-scale convergence of the compressible Reynolds lubrication equation modeling the flying characteristics of a rough magnetic head over a rough rigid-disk surface*, ESAIM Math. Model. Numer. Anal., **29** (1995) 199–233.

[17] R. Kornhüber, *Monotone multigrid methods for elliptic variational inequalities I*, Numer. Math., **69** (1994) 167–184.

[18] C. A. Lacey, F. E. Talke, *A tightly coupled numerical foil bearing solution*, IEEE Transactions on Magnetics, **26** (1990) 3039–3043.

[19] E. Marusić-Paloka, M. Starcevic, *Derivation of equations for gas lubrication via asymptotic analysis of the compressible Navier-Stokes system*, Nonlinear Analysis: Real World Applications, **11** (2010) 4565–4571.

[20] U. Trottenberg, C. W. Oosterlee, A. Schüller, *Multigrid*, Academic Press, 2001.

[21] C. H. Venner, A. A. Lubrecht, *Multilevel Methods in Lubrication*, Tribology Series, 37. Elsevier, Amsterdam, 2000.

[22] L. Wu, D. B. Bogy, *Numerical solution of a slider air bearing problem of hard disk drives by two multidimensional upwind residual distribution schemes over unstructured triangular meshes*, Journal of Computational Physics, **172** (2001) 640–657.

[23] Y. Wu, F. E. Talke, *A finite element simulation of the two-dimensional head/tape interface for head contours with longitudinal blend slots*, Tribology Internat., **33** (2000) 123–130.